



A stochastic framework for uncertainty analysis in electric power transmission systems with wind generation

Giovanni Sansavini, Roberta Piccinelli, L. R. Golea, Enrico Zio

► To cite this version:

Giovanni Sansavini, Roberta Piccinelli, L. R. Golea, Enrico Zio. A stochastic framework for uncertainty analysis in electric power transmission systems with wind generation. *Renewable Energy*, 2014, 64, pp.71-81. 10.1016/j.renene.2013.11.002 . hal-00926356

HAL Id: hal-00926356

<https://hal-centralesupelec.archives-ouvertes.fr/hal-00926356>

Submitted on 9 Jan 2014

HAL is a multi-disciplinary open access archive for the deposit and dissemination of scientific research documents, whether they are published or not. The documents may come from teaching and research institutions in France or abroad, or from public or private research centers.

L'archive ouverte pluridisciplinaire **HAL**, est destinée au dépôt et à la diffusion de documents scientifiques de niveau recherche, publiés ou non, émanant des établissements d'enseignement et de recherche français ou étrangers, des laboratoires publics ou privés.

A stochastic framework for uncertainty analysis in electric power transmission systems with wind generation

(G. Sansavini^a, R. Piccinelli^a, L. Golea^a, E. Zio^{b,a,*})

^aPolitecnico di Milano, Energy Department, Nuclear Section, c/o Cesnef, via Ponzio 33/A, 20133, Milan, Italy

^bChair on Systems Science and the Energetic challenge, European Foundation for New Energy-Electricite' de France Ecole Centrale Paris and Supélec, Grande Voie des Vignes, F92-295, Chatenay Malabry Cedex

*corresponding author

enrico.zio@ecp.fr, enrico.zio@polimi.it

Abstract

The purpose of this work is the analysis of the uncertainties affecting an electric transmission network with wind power generation and their impact on its reliability. A stochastic model **was developed to simulate** the operations and the line disconnection and reconnection events of the electric network due to overloads beyond the rated capacity. We represent and propagate the uncertainties related to consumption variability, ambient temperature variability, wind speed variability and wind power generation variability. The model is applied to a case study of literature. Conclusions are drawn on the impact that different sources of variability have on the reliability of the network and on the seamless electric power supply. Finally, the analysis enables identifying possible system states, in terms of power request and supply, that are critical for network vulnerability and may induce a cascade of line disconnections leading to massive network blackout.

1. Introduction

Systems of electric power generation, supply and transmission play an extremely important role in modern societies. Consumers have grown to expect electricity to be available instantaneously “with a flick of a switch”, because their lives depend on seamless electric power supply as an essential resource for communication, transportation, heating and cooling systems, lighting, and the powering of computers and electronics.

Providing electricity in a reliable fashion is a complicated and technically challenging task. It involves real-time assessment, coordination and control of thousands of generating units, the transfer of electric power over networks of transmission lines and, finally, the delivery of electric power to the consumers. The high degree of inter- and intra-connectedness of networks for energy supply makes them vulnerable to global disruptions when exposed to hazards of various nature, from random/mechanical/physical/material failures to natural events, intentional malevolent attacks, and human errors [1].

The assessment of power system reliability is generally divided into two aspects: system adequacy and system security [2]. System adequacy deals with steady-state operation and planning of the power system, i.e., it gauges the ability of a power system to supply and deliver electric energy to satisfy customer demand. System security gauges the ability of a power system to respond to sudden changes or disturbances such as the loss of generators or transmission lines. Power system security involves two aspects. The first is related to the ability of the system to withstand internal failures and sudden natural disturbances, including network overload, voltage problems, and instability problems. The second aspect is related to the ability of the system to avoid external interference, attack, or coordinated physical assault on the system. Traditionally system planners deal only with the former security aspect, i.e., problems arising from system operation, random failures of system equipment and natural disturbances [3].

The overarching goal of electric resource planning is therefore to ensure that sufficient resources, delivery capacity, and reliability characteristics exist to meet future demand requirements in a reliable and economic manner [4]. All resource planners allow some percentage reserve margin of capacity above their demand requirements to ensure reliability following unexpected system conditions and to meet state regulatory and regional requirements. Reserve margins are determined by calculating the capacity of supply resources, discounted to reflect the potential unavailability of the resources at high risk times [3].

The analytical processes used by resource planners range from relatively simple calculations of planning reserve margins to rigorous reliability simulations that quantify system Loss of Load Expectation (LOLE) or Loss of Load Probability (LOLP) values. In the latter case, planners periodically check resource adequacy indicated by the evaluated reserve margins through detailed reliability simulations that compare expected demand profiles against forced outage rates of generating units and maintenance schedules to yield LOLE or LOLP values [2, 5]. Moreover, reliability calculations typically include probabilistic production cost simulations for meeting a specified demand (or chronological) curve from a specified generation fleet while incorporating the forced and unforced outage rates over the simulation period.

Deterministic approaches to power system security usually consider worst-case scenarios. The result of the analysis is most often qualitative and therefore difficult to use in a decision-making process. Deterministic methods also impose a hard limit on system operations. As a result, systems are often designed, planned or operated to withstand severe problems that have a low probability of occurrence.

Deterministic methods alone cannot adequately address the various transmission challenges such as the available transfer capability (ATC), long transmission and related voltage/reactive and security (stability) problems, transmission project ranking, transmission congestion alleviation, uncertainty of weather, environmental constraints and the competitive environment, uncertainty of customer load demand, uncertainty of equipment failure and operation.

Probabilistic approaches consider factors that may affect the performance of the system and provide a quantified risk assessment using performance indices such as probability and frequency of occurrence of an

unacceptable event, its duration and severity. These performance indices are sensitive to factors that affect system reliability. Quantified descriptions of the system performance, together with external relevant factors such as environmental impact, social and economic benefits etc., enter into the decision-making process and have an impact on operations, short-term planning and long-range planning [3]. These assessments are traditionally carried out by Monte Carlo simulation techniques [6, 7, 8], and by analytical methods [9]. Uncertainty and fast fluctuation of wind speeds strongly affect system planning and operation and call for effective reliability-based reserve expansion. With respect to this key issue, analytical methods are applied in [9], where universal generating functions are employed to quantify the impact of high wind power penetration on the system reserve and reliability from long-term planning point of view. The impact of transmission network on customers' reliabilities is also considered.

In this paper, the reliability of a power transmission network is addressed in the face of uncertainties related to consumption variability, ambient temperature variability, wind speed variability and the integration of large shares of electricity produced by wind energy. The proposed simulation framework combines classical DC power flow, sequential Monte Carlo sampling of the possible uncertain system parameters, and a model for power line disconnection and reconnection due to line overloading beyond the rated capacity. Within this simulation framework, the uncertainties related to consumption, wind power generation, ambient temperature and wind cooling of lines are identified, and they are quantitatively propagated to assess their impact on level II system adequacy [2] in terms of expected energy not served (EENS) and expected demand not supplied (EDNS). Based on the aforementioned modeling, it can be anticipated that the parameters whose uncertainty affects power system operations to a large extent, will have to be paid special attention during the design and management of power systems. Finally, critical system states of wind power generation and load request that may lead to a cascade of line disconnection and a large system blackout are pointed out.

The paper is organized as follows. In Section 2, the power grid DC load flow, the wind turbine and the line overload models which enter the stochastic simulation framework are detailed. In Section 3, the uncertainties related to power system operations are identified and quantitatively represented. In Section 4, the developed framework is exemplified with respect to a modified version of the IEEE RTS 96 test network system [10], and reliability and vulnerability considerations about network operations are provided. Conclusions are drawn in Section 5.

2. Stochastic Modeling Framework of a Power Transmission System

In order to study the effects of the uncertainties (related to the load and the renewable generation forecasts on one side, and to weather parameters on the other side) that introduce disturbances in the grid and may cause line outages due to overloads, an event-based stochastic framework which simulates the operations of the electric network under variable conditions was developed. The proposed approach, inspired by the model introduced in [11, 4, 12, 13], combines: 1) a DC load flow algorithm that computes the distribution of power

flow using a linear load flow approximation, 2) the contribution of wind generation power in a transmission power grid, 3) a strategy for generation dispatch in order to balance the power production and consumption throughout the network, 4) the dynamics of line temperatures as function of the power flow and environmental conditions (wind speed and ambient temperature), 5) the event of automatic line disconnection when the rated line temperature is reached, and 6) the event of line reconnection.

The evolution of cascading events in their slow initiating stages is represented by transmission lines failures, caused by overheating due to excessive power flows. To describe this effect, the evolution of the line temperature and its dependence on electric flow redistributions was modeled using the model of heat conduction in rods of small cross section in which an electric current of constant intensity flows [12]. Further contributing to the evolution of cascades is a line restoration model which prevents a damaged line to be put back in service before a fixed restoration time has passed. Random failures of transmission lines during normal operations may also contribute to the evolution of cascading events. The occurrence of a random failure can be straightforwardly introduced in the developed event-based stochastic model. However, given the small value of random failure rates for transmission equipment, multiple, independent line failures scarcely affect the evolution of the cascade process. At the same time, single line failures due to random events have little impact in an $N-1$ compliant transmission system. With no loss of generality, random failures of transmission lines during normal operations are not included in the model at its current stage for the sake of a clearer quantification of the other sources of uncertainty in the system.

The model of transmission line failure due to loading over their transmission capacity and following restoration, is part of the developed event-based stochastic framework which has also the ability to represent daily hourly changes in power requests at customer side of the system, ambient temperature and wind speed variations.

The stochastic framework is based on sequential Monte Carlo Simulation (MCS) in which the combination of load requests, ambient temperature, wind power generation, wind speed and network topology is a system realization. Due to the yearly periodicity of the load request and the room temperature average values, each year is considered to be statistically equivalent to one another and the results are provided on the basis of yearly averages. The simulation begins by establishing the load demand, the room temperature and wind speed values. If no line disconnection due to excessive heating occurs, the next event corresponds to the occurrence of the next hourly time step (“next hour” event) with updated load demand, ambient temperature and wind speed conditions. If the temperature of a line exceeds the critical temperature set for that line, a “line disconnection” event may occur before the scheduled “next hour” event. A DC load flow is performed following the occurrence of each event. The “line reconnection” event occurs after a time chosen a priori for each line that is disconnected.

After each event, we solve the DC load flow equations in order to determine the line temperatures and the type of the next event. The change time to the next event is computed as the minimum between the time to

the next hour change, the minimum failure time among all lines and the minimum time to reconnection of all lines.

A. Formulation of the DC power flow

The electrical transmission system is assumed to operate through steady-state conditions, also during the evolution of major disturbances in the system. This approximation does not hold during the late stages of major disturbance events and it can be relaxed if voltage dependent phenomena are modeled during these events.

In order to determine the steady-state operating conditions of the power grid, the full nonlinear power flow equations that provide information about the voltage magnitudes and phases and the active and reactive power flows along each transmission line should be solved. Unfortunately, since the simulations involve numerous power flow solutions for a power grid system that evolves in time, solving repeatedly the full nonlinear power flow equations becomes computationally prohibitive. Moreover, the full nonlinear equations pose very difficult nonlinear optimization problems. Therefore, the power-flow equations are linearized into the so-called DC power flow equations that connect the flow of real power to the voltage phases of the system buses, which results in a completely linear, non iterative, power flow algorithm [14].

The DC power flow can only calculate real (MW) flows on transmission lines but it gives no answers to what happens to voltage magnitudes or reactive (MVAR) flows. Assuming that all bus voltages phasors are 1.0 per unit in magnitude, and defining the matrix B by $B_{ij} = -b_{ij}$ and $B_{ii} = \sum_j b_{ij}$, where b_{ij} is the susceptance of the transmission line joining buses i and j and the summation is over all nodes j connected to node i , the voltage phases θ_i are the solution of the linear power flow equation $P = B\Theta$. Here, P is the vector whose $N - 1$ components are the real powers injected at each node, except a reference node (slack node) for which the injected real power is computed from the power balance between total generation and total load. The vector Θ is the vector whose components are the voltage phases at each node in the network except the slack node which has phase zero. After solving the power flow equation for the vector Θ , the flow of real power along each transmission line is computed from $P_{ij} = b_{ij}(\theta_i - \theta_j)$ [15].

B. Line temperature model and overloaded-line failure

In order to model the failure of transmission lines due to loading beyond the rated transmission capacity, the problem of heat conduction is analyzed for rods of small cross-section [16] in which an electric current of constant intensity flows. For simplicity, the transmission line is assumed to be so thin that the temperature at all points of its cross-section is uniform. The transmission line is supposed to have constant cross-section area ω , perimeter p , thermal conductivity K , electrical conductivity σ , density ρ , specific heat c , diffusivity κ . It is also assumed that the heat flux across the surface of the line is proportional to the temperature difference between the surface and the surrounding medium and is given by $H(T - T_0)$, where T is the

temperature of the line, T_0 is the temperature of the medium and H is the surface conductance. The problem of heat conduction, then, becomes one of linear heat flow in which the temperature is specified by the time t and the distance x measured along the transmission line. Balancing the total heat generation in an element of volume bounded by the cross sections at x and $x+dx$ and the heat in flow across the surface minus the heat loss at the surface, we write the following heat equation,

$$\frac{\partial T(x,t)}{\partial t} = \kappa \frac{\partial^2 T(x,t)}{\partial x^2} + \alpha I^2 - \nu(T(x,t) - T_0) \quad (2.3)$$

where $\nu = Hp / (\rho c \omega)$, $\alpha = 0.239 / (\rho c \omega^2 \sigma)$, $\kappa = K / (\rho c)$ and $I = P/V$ is the current in the line measured in Amperes [16]. In order to estimate the surface conductance H , it is assumed that the loss of heat across the surface of the line is due to forced convection. When fluid (gas or liquid) at temperature T_0 is forced rapidly past the surface of the line, it is found experimentally that the rate of loss of heat from the surface is given by $H(T - T_0)$, with a value of the coefficient H which depends on the velocity and the nature of the fluid and the shape of the surface [16]. For turbulent flow of air with velocity u perpendicular to a circular cylinder of diameter d , $H = 8 \times 10^{-5}(u/d)^{1/2} \text{ cal/(cm}^2\text{secK)}$.

Assuming that fluctuations in power flows along the transmission lines propagate much faster than any heat flow transients, and since the heat source is equally distributed along the line, we can neglect the spatial variation in temperature along the line in order to get this simple equation describing the time evolution in the temperature of the line with the time evolution of the power flowing through the line:

$$\frac{\partial T(x,t)}{\partial t} = \alpha I^2 - \nu(T - T_0) \quad (2.4)$$

If the line is initially at temperature $T(0)$ and the power flowing through the line has the constant value P , the line temperature evolves according to this simple equation:

$$T(t) = e^{-\nu t} (T(0) - T_e(P)) + T_e(P), \quad (2.5)$$

where

$$T_e(P) = \frac{\alpha}{\nu} \frac{P^2}{I^2} + T_0, \quad (2.6)$$

is the equilibrium temperature that the line reaches at $t \rightarrow \infty$. If at some moment the power flow changes, we reset the clock and the initial temperature, and use the same equation to describe the evolution of line temperature starting from this moment on.

A transmission line failure due to excessive heating, followed by line sagging and tripping, will occur if the power flow through it exceeds the maximum line rating. For each line l , we denote by T_{cl} the equilibrium temperature corresponding to a constant power flow equal to the line rating P_l^{\max} , i. e. $T_{cl} = T_e(P_l^{\max})$. When the power flow P_l through the line changes up to exceeding P_l^{\max} , the line will start heating, with the

temperature increasing towards the equilibrium temperature corresponding to the new power flow. Since this equilibrium temperature exceeds T_{cl} , at some time t_{cl} the line temperature will reach T_{cl} and the line will fail. The failure time, t_{cl} , measured from the moment when the grid topology and the line flow has changed, can be easily deduced from Eq. (2.5) and is given by

$$t_{cl} = \frac{1}{\nu} \ln \frac{T_{cl} - T_e(P_l)}{T(0) - T_e(P_l)} \quad (2.7)$$

Finally, in order to keep the heat equation linear, we have omitted on the right-hand side of Eq. (2.3) a cooling term that takes into account that each element of the surface of the road loses heat by radiation to the surrounding medium — and provides cooling when the wind is absent.

Figure 1 shows the dynamics of the power flows (thin curve) and temperatures (thick curve) for one transmission lines during the simulated operations of a power grid. We can see that line temperature reaches its threshold value at about $t = 8467$ hours due to excessive line flow (beyond scale in Figure 1). When the threshold temperature is reached, the line is isolated and the electric flow rapidly drops to 0 MW, followed by line temperature decay to the room temperature by heat convection through the line surface. The line is assumed to be put back in service after 10 hours and the electric flow is restored.

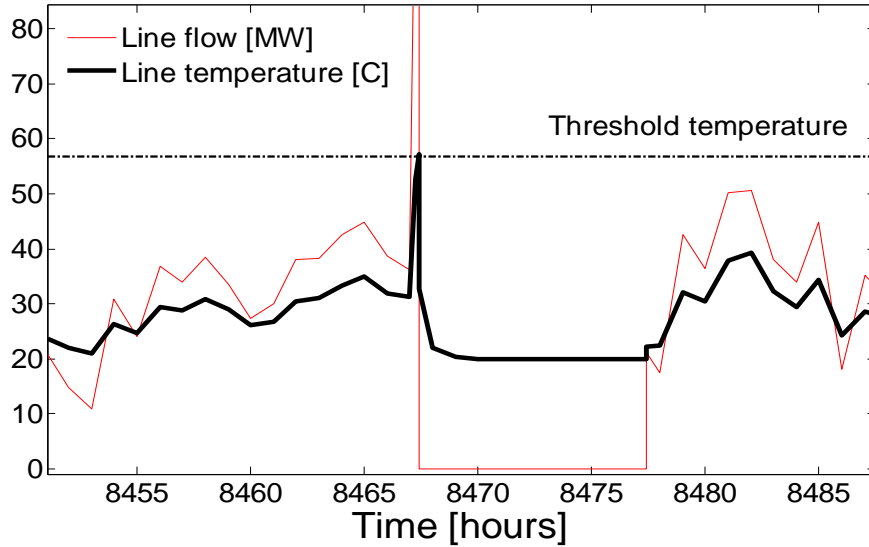


Figure 1. Dynamics of power flow and temperature for a transmission line during network operations

C. Wind turbine model

The power output from a wind turbine generator (WTG) is determined using the functional relationships linking the characteristics of a WTG and the wind speed field [13]. This function is described by the operational parameters of the WTG. The parameters commonly used are the cut-in wind speed V_{ci} (at which

the WTG starts to generate power), the rated wind speed V_r (at which the WTG generates its rated power) and the cut-out wind speed V_{co} (at which the WTG is shut down for safety reasons). Equation (2.1) [13] is used to obtain the power output of a WTG from wind speed (SW_t):

$$P(SW_t) = \begin{cases} 0 & 0 \leq SW_t \leq V_{ci} \\ (A + B * SW_t + C * SW_t^2) * P_r & V_{ci} \leq SW_t \leq V_r \\ P_r & V_r \leq SW_t \leq V_{co} \\ 0 & SW_t \geq V_{co} \end{cases} \quad (2.1)$$

The constants A, B, C depend on V_{ci} , V_r and V_{co} as expressed in eq. 2.2:

$$\begin{aligned} A &= \frac{1}{(V_{ci} - V_r)^2} \left\{ V_{ci} (V_{ci} + V_r) - 4V_{ci} V_r \left[\frac{V_{ci} + V_r}{2V_r} \right]^3 \right\} \\ B &= \frac{1}{(V_{ci} - V_r)^2} \left\{ 4(V_{ci} + V_r) \left[\frac{V_{ci} + V_r}{2V_r} \right]^3 - (3V_{ci} + V_r) \right\} \\ C &= \frac{1}{(V_{ci} - V_r)^2} \left\{ 2 - 4 \left[\frac{V_{ci} + V_r}{2V_r} \right]^3 \right\} \end{aligned} \quad (2.2)$$

Figure 1 presents the output power of a WTG:

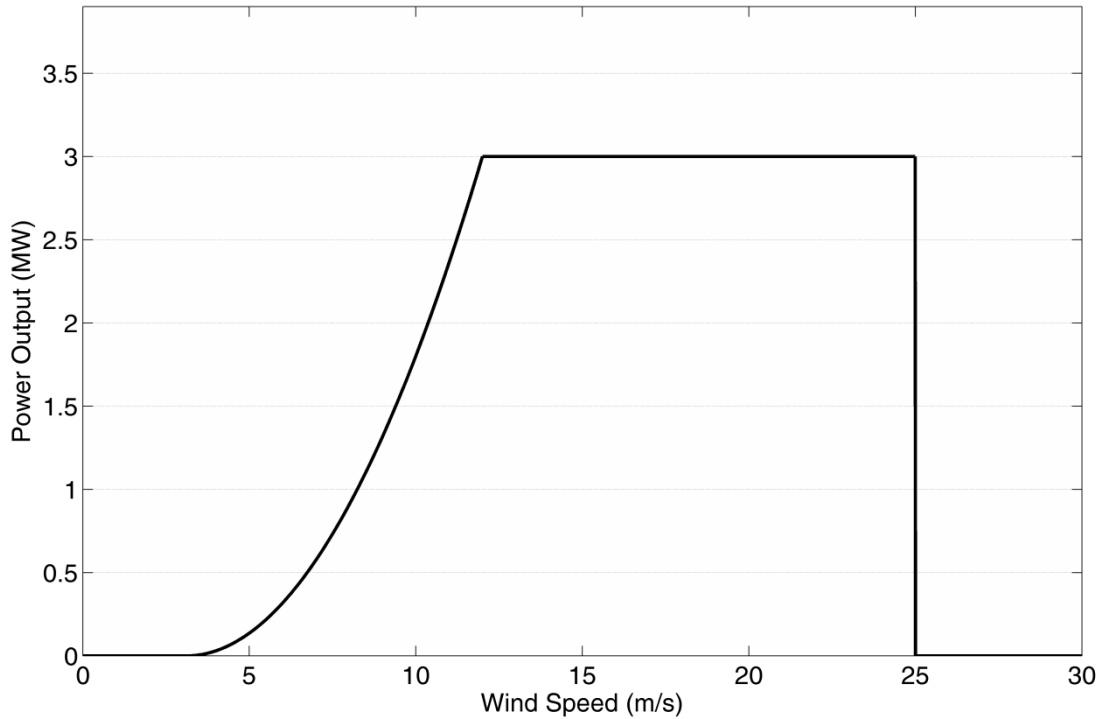


Figure 2. Power curve of a WTG with the following parameters: rated power P_r of 3 MW, cut-in speed, V_{ci} , of 3ms^{-1} , rated speed, V_r , of 12ms^{-1} and cut-out wind speed, V_{co} , of 25ms^{-1}

The wind turbine generating unit operates in four phases: a first standby phase in which wind speed is lower than $V_{ci} = 3 \text{ ms}^{-1}$ and there is no power production; a second phase in which power production increases with a nonlinear trend in the wind speed range from $V_{ci} = 3 \text{ ms}^{-1}$ to $V_r = 12 \text{ ms}^{-1}$; wind turbines usually reach the rated power at a wind speed between 12 ms^{-1} and 16 ms^{-1} , depending on the design of the individual turbine; finally, when the wind speed exceeds the rated wind speed, the wind generator is disconnected for protection purposes and the power production stops (cut-off phase). Hence, a wind turbine produces its maximum power, i.e. the rated power, within a certain interval that has its upper limit at the cut-out wind speed. Typical values of the cut-out wind speed range between 20 ms^{-1} and 25 ms^{-1} [17].

3. Identifying and Classifying Uncertainties in Power Transmission Systems

One of the main purposes of a power system is to satisfy the demands of customer loads in a reliable and economical manner. Failing to properly address planning problems and constraints will eventually yield operation problems and, therefore, will affect power system reliability. Variability in demand, transmission and generation parameters, line ratings, extreme weather, and other environmental factors, introduce uncertainty in operation and planning of electric networks. In general, the degree of uncertainty increases significantly from a shorter time frame in system planning to a longer time frame in system operation. Failing to incorporate uncertainties in system planning may lead to an overestimation of safety margins and of system capabilities to maintain acceptable levels of reliability. Therefore, it is of paramount importance to identify and quantify the sources of uncertainty in electric networks.

Indeed, the appropriate incorporation of the uncertainty and the presentation of its implications are widely recognized as fundamental components in the analyses of complex electric systems [18]. There are two different forms of uncertainty in power system reliability assessment [19]. On the one hand, aleatory uncertainty arises because the system can stochastically behave in different ways. Components' failures and repair processes are random and are sources of aleatory uncertainty. On the other hand, uncertainty enters the system reliability assessment due to incomplete knowledge and information on the system and its related phenomena, which leads to imprecision in the model representation of the system and in the evaluation of the system parameters. This latter type of uncertainty is often referred to as subjective, epistemic, state-of-knowledge [20]. For example, in the field of power system research, epistemic uncertainty has been dealt within the fuzzy power flow analysis [21; 22], where the power injections of all loads and generations are regarded as fuzzy variables.

Table I summarizes the uncertainties identified in the electrical transmission system. In this study, we represent and propagate the uncertainties related to (I) consumption variability, (II) ambient temperature variability, (III) wind speed variability and (IV) wind power generation.

<i>Element</i>	<i>Parameter</i>		<i>Source of uncertainty</i>	<i>Type of available information</i>	<i>Uncertainty representation</i>
Load bus	Load value		Consumption variability	Historical data	Probabilistic (Normal pdf)
Wind generating unit	Output power	Wind speed	Wind speed variability	Historical data	Probabilistic (Weibull pdf)
		Operation parameters	Wind power variability	Experimental data	Probabilistic (Normal pdf)
Weather	Wind speed		Wind speed variability	Historical data	Probabilistic (Weibull pdf)
	Ambient temperature		Temperature variability	Historical data	Probabilistic (Normal pdf)
Transmission Line	Line temperature		Material properties incomplete knowledge	Experts' judgment	Possibilistic

Table I. Uncertainty sources and their representation in the electrical transmission system

When the uncertainty in the variables is mainly due to their inherent randomness (aleatory uncertainty) and there is sufficient information to assign probability distributions and estimate their parameters, probabilistic modeling is embraced. The model output is represented by a function of n random variables, $Y = f(X_1, \dots, X_i, \dots, X_n)$, where X_i denotes the i -th probabilistic input variable with PDF $p_{x_i}(x)$. The probabilistic model defines the probability distribution of the output random variable Y as a function of the probability distribution of the inputs. Such distribution is evaluated analytically in simple cases, or by Monte Carlo Simulation (MCS) for more realistic settings.

In power system studies, the MCS is typically embraced, given the large number of variables involved and their complex relationships, which make analytical models difficult or even impossible to derive [23; 24]. The operative procedure of MCS calls for a large number m of iterations: at each e -th iteration, an input vector of values $(x_1^e, x_2^e, \dots, x_n^e)$ is sampled from the probabilistic density functions (PDFs) of the input variables and a realization of the output value y^e is computed solving the system model. After m repetitions, an empirical estimate of the distribution of the system output is obtained.

3.1 Uncertainty representation of the power demand at load buses

The average hourly peak power demand follows the hourly load curve based on data from [10]. The curve accounts for customer power need variations from day to night and from season to season. An example of a daily load peak curve, in different days and seasons, is given in Figure 3.

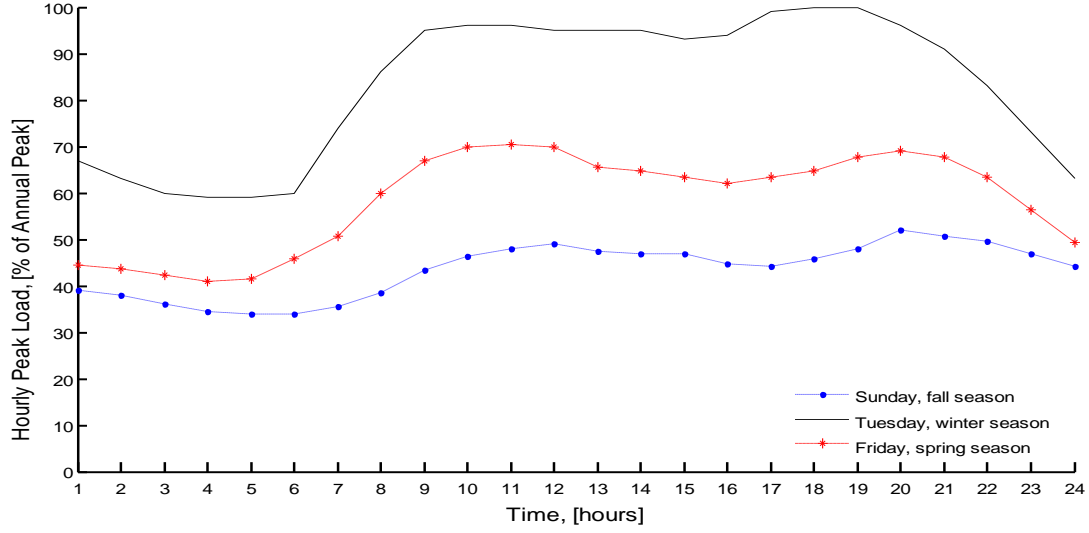


Figure 3. 24-hours load curve [10]. First hour corresponds to 12 a.m. – 1 a.m. interval of each day

Variability in the hourly peak power demand arise because power consumption by users is not exactly uniform and simultaneous, i.e. **it is assumed** that the power needed at the customers side may experience stochastic fluctuation from the average hourly peak power demand. Following [2], it is assumed that load uncertainty is well described by a normal distribution. Therefore, the load hourly values are sampled from a normal distribution $N(\mu, \sigma^2)$ with mean μ equal to the hourly peak load considered in the deterministic case (Fig.3) and standard deviation σ assigned according to the perceived load forecast uncertainty, such as 10% of the mean value, $\sigma = 0.1\mu$ [2].

3.2 Uncertainty representation of the ambient temperature

In order to compute the annual ambient temperature curve (Fig.4), the daily minimum and maximum values during one year in a specific location of the United States were collected and analyzed. A linear variation of the temperature values between the daily minimum and maximum values is assumed, with the minimum and maximum peak registered at 5 a.m. and 4 p.m., respectively.

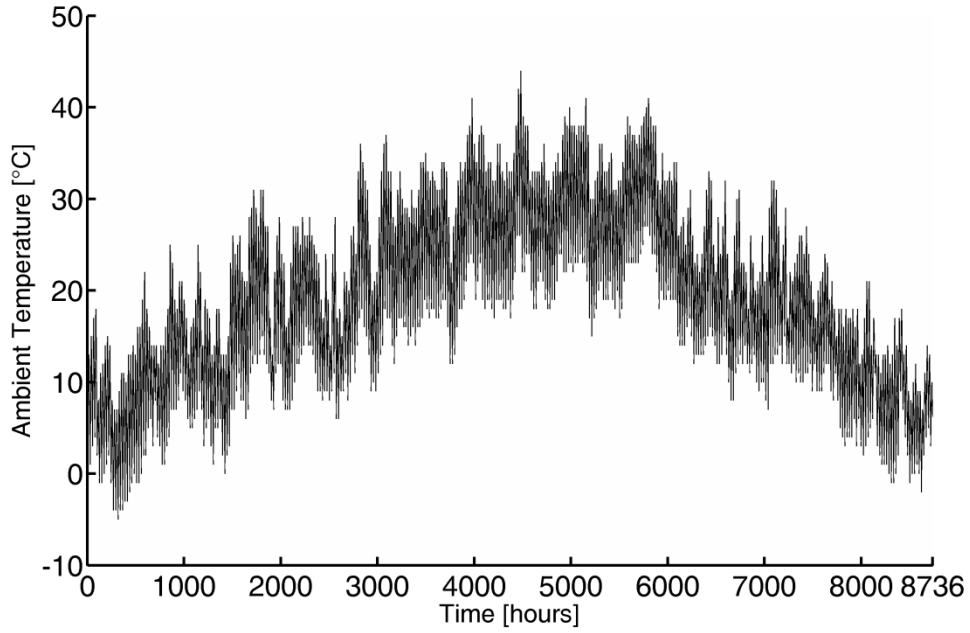


Figure 4 Ambient temperature curve used in the deterministic case. The maximum and minimum data values have been collected at the location of Bakersfield, CA, USA.

The uncertainty associated with the ambient temperature **is assumed to be well** described by a normal distribution. Therefore, the temperature hourly values are sampled from a normal distribution $N(\mu, \sigma^2)$ with mean μ equal to the hourly value from the annual ambient temperature curve (Fig. 4) considered in the deterministic case and standard deviation σ equal to 5% of the mean value, $\sigma = 0.05\mu$. This value has been identified by computing the standard deviations of the minimum of the median and of the maximum temperature values that are recorded within each month of the year by choosing the maximum among them.

3.3 Uncertainty representation of the wind speed

In order to compute the annual wind speed curve, the hourly values during a year in a specific location were collected and analyzed. In the deterministic case it is assumed, for each day of the year, that the wind speed is constant throughout the day and it is equal to the daily average value.

Following [25; 26], the Weibull distribution has been used to represent the wind speed variability within a yearly time frame. It is shown that data collected at many locations around the world can be reasonably well described by the Weibull PDF if the collection time frame is not too short, i.e. longer than several weeks. Figure 5 shows the distribution of the hourly wind speed collected at Bakersfield, CA, USA, and the Weibull distribution whose parameters are calculated by maximum likely estimation [25] based on the hourly values. From the collected data, **it can be noticed** that either the used anemometer has a lower bound of measuring at about roughly 6 ms^{-1} , or a wind speed below 6 ms^{-1} is an unlikely event at the considered location. Moreover, **it can be noticed** that the Weibull approximations holds beyond the maximum of the distribution while it is a rough approximation for lower speed values [27]. Therefore, **it may be expected** that the wind speed values

sampled from the Weibull distribution will be biased towards lower values if compared to the collected data. Nonetheless, this bias does not affect the modeling framework that is the main objective of the work.

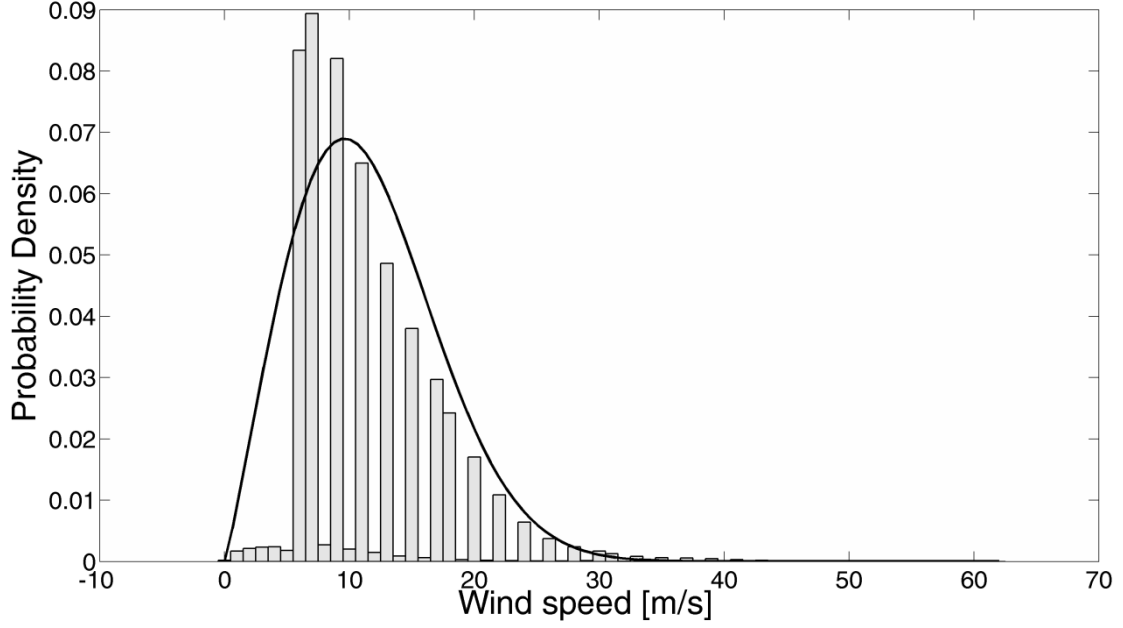


Figure 5. Distribution of the wind speed values collected at Bakersfield, USA, and the corresponding Weibull distribution evaluated through maximum likelihood estimation of the distribution parameters.

3.3 Uncertainty representation of the wind power generation

Finally, the variability of wind speed propagates to the power output of wind generators. The power output of a WTG depends strongly on the wind regime as well as on the performance characteristics and the efficiency of the generator. A fundamental assumption is made when considering the deterministic power curve (Figure 2): the relationship between the wind speed and the output power is fixed, given the same type of WTG systems. In other words, the output power of the WTG is always the same at a specific wind speed. In reality, the output power for a fleet WTG of the same type always exhibits considerable variations even when they are operating at the same wind speed [28]. Moreover, Thiringer and Linders [29] analyzed the relationship between the wind speed and the output power based on a group of wind turbines. They found that the powers generated from individual wind turbines of the same type actually vary even at the same wind speed. These research findings suggest that a probabilistic model incorporating the power variations may be more appropriate to characterize the relationship between the wind speed and the actual output powers. Following [30], the actual output power P_d is proposed as a random variable, which is characterized by the mean power output and its standard deviation:

$$P_d(x) = P(x) + \varepsilon \quad (2.8)$$

where $P_d(x)$ represents the actual WTG power output, $P(x)$ represents the deterministic output governed by the equation (2.1) and ε represents the variation of the power output with $\varepsilon \sim N(0, \sigma_\varepsilon^2)$. Following [30], $\sigma_\varepsilon = 0.1 \cdot P_r$, i.e. 10% of the rated power output. Since the uncertainty in wind speed is also modeled, the function for power curve actually contains two random parameters: the wind speed $x \sim \text{Weibull}$ and the variation of the power output $\varepsilon \sim N(0, \sigma_\varepsilon^2)$.

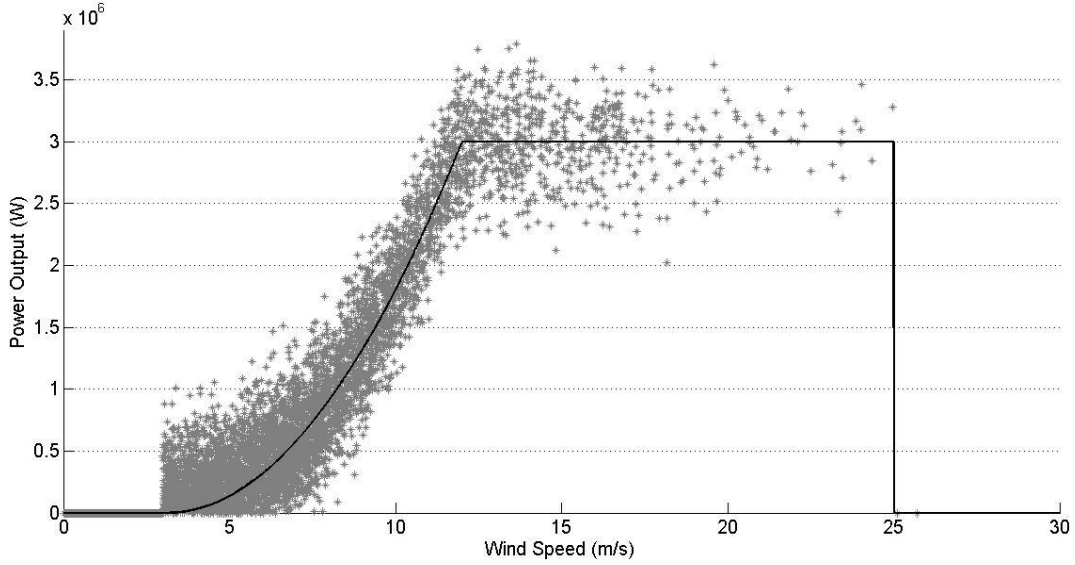


Figure 6. Power output realizations for the wind regime described by the Weibull distribution of Figure 5, and the performance characteristic and efficiency of the generator.

Figure 6 shows the power output realizations (grey points) of the WTG of Figure 2 for the wind regime described by the Weibull distribution of Figure 5, and the performance characteristics and efficiency of the generator described by $N \sim (0, \sigma_\varepsilon^2)$ [29]. The wind turbine starts producing power when wind speed equals the cut-in speed of 3 ms^{-1} : the majority of wind power generation concentrates during the nonlinear part of the output curve. This effect is consistent with the uncertainty in wind speed distribution.

4. Application to a modified version of IEEE RTS 96 [10]

The composite test system IEEE-RTS (Fig. 7) was modified to exemplify the stochastic framework in Section 2 with respect to a test system that reproduces the general conditions that exist in actual power systems. The original RTS has a very strong transmission network and a weak generation system. Following [31], in this paper the original RTS is modified to create a more practical system with a relatively weaker

transmission network and a relatively stronger generation system with respect to the original IEEE-RTS test system.

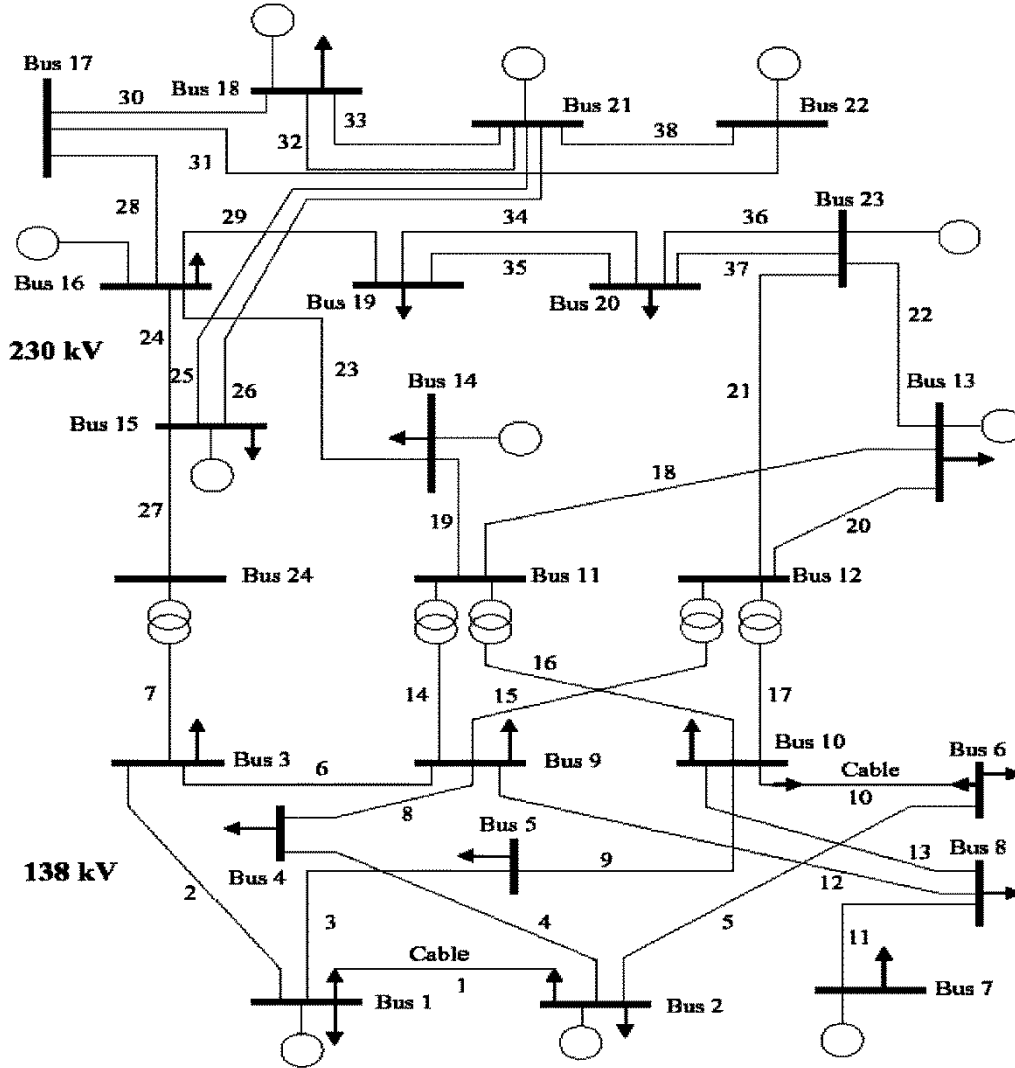


Figure 7. The single line diagram of the IEEE RTS 96/MRTS scheme [10; 31]

The total installed capacity in the original RTS is 3405 MW in 32 generating units and the peak load is 2850 MW. In the modified version of RTS, henceforth designated as the MRTS, the lengths of all the 138-kV lines (lower part of the system in Figure 7) are doubled except for line 10 which is 25.6-km cable. The 230-kV lines (the upper part of the system in Figure 7) are extended as follows: the lengths of lines L21, L22, L31, L38 are increased by a factor of three; the lengths of lines L18 to L20, L23, L25 to L27 are increased by a factor of four; the lengths of lines L24, L28 to L30, and L32 to L37 are increased by a factor of six. To increase the utilization of the transmission network, the load levels at all delivery points were increased from 1.3 p.u. to 1.5 p.u. of the original values. The increase of the load levels is balanced by doubling the generating systems capabilities at Buses 16, 18, 21, 22 and 23. The total number of generating units is now 44. The total system capacity is 5320 MW and the peak load for the different load levels is given in Table II.

Load level (p.u.)	Peak load [MW]
1.3	3705
1.4	3990
1.5	4275

Table II. Load levels and corresponding peak loads for the modified power grid MRTS.

The single line diagram of the MRTS is the same as that of the unmodified version of RTS shown in Figure 7. Following the aforementioned modifications, the transmission utilization in the MRTS is significant, as a considerable amount of power is transferred from the northern to the southern portion of the system. The modified system is used as a test bed to examine also the effects of uncertainties introduced by adding wind energy conversion systems (WECS) in two points of the transmission network: two additional 300 MW WECS are added through transmission lines at Buses 1 and 3 in the southern portion (138 kV) of the MRTS (Fig. 8).

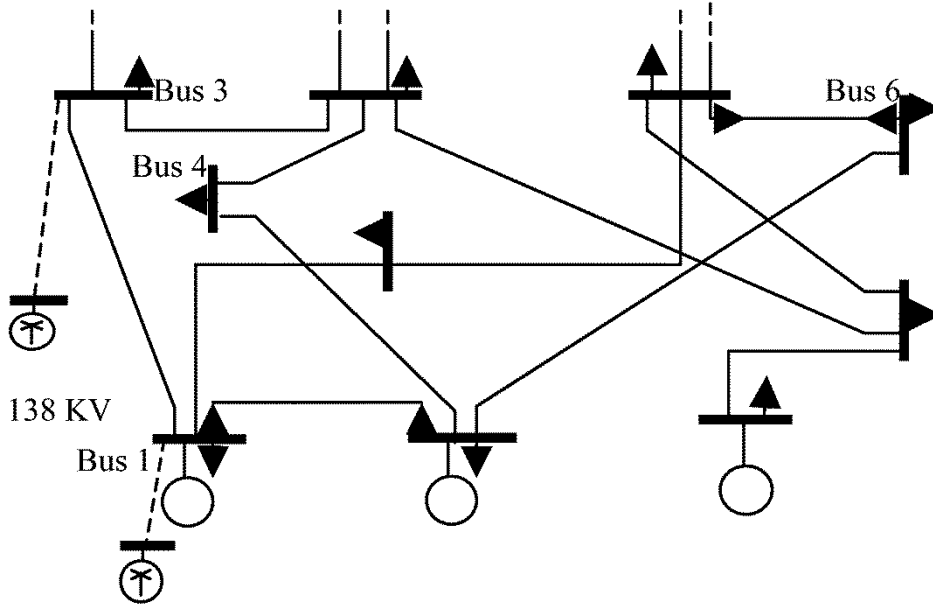


Figure 8. The two 300 MW WECS at Buses 1 and 3 in the MRTS [31].

For each load level in Table II, four different scenarios are assessed in order to observe the effects of uncertainties, and compared to the deterministic base case scenario in which uncertainty is neglected. In order to keep the comparisons consistent, the deterministic base case scenario is characterized by hourly variability of load, hourly variable ambient temperature, and a mean wind speed value which follows the

hourly average values, with no associated uncertainty; the additional generators of 300 MW each, are supposed to have no uncertainty associated to their power production.

Following the uncertainty models described in Section 3, the first three scenarios deal separately one uncertainty at a time, with uncertainties in load demand (scenario I), uncertainty in ambient temperature (scenario II), and uncertainties in wind speed and power generation (scenario III). The fourth scenario combines the effects of all the uncertainties (scenario IV). The sensitivity of the annual energy loss with respect to customers power requests, ambient temperature, wind speed, and wind power generation were quantified and reported in Table III.

The annual energy loss is quantified by the Expected Energy Not Supplied, i.e. the average EENS index. The EENS index is an adequacy index for the transmission level of the electric infrastructure [2]. It quantifies the annual electric energy that could have been provided by the generating system but that could not reach the customers due to bottlenecks in the transmission network.

Load Level = 1.3 (p.u.)	Annual Energy Loss EENS[MWh]	
	Mean	Standard deviation
Base Case	-	-
Uncertainty in load demand	85.217	11.523
Uncertainty in ambient temperature	61.574	5.779
Uncertainty in wind speed and power	393.50	19.57
Uncertainty	438.99	17.52

Load Level = 1.4 (p.u.)	Annual Energy Loss EENS[MWh]	
	Mean	Standard deviation
Base Case	2.0872e+003	-
Uncertainty in load demand	2.6895e+004	3.7602e+003
Uncertainty in ambient temperature	3.6079e+003	3.9286e+001
Uncertainty in wind speed and power	1.0116e+004	8.6805e+001
Uncertainty	9.8776e+003	7.4779e+001

Load Level = 1.5 (p.u.)	Annual Energy Loss EENS [MWh]	
	Mean	Standard deviation
Base Case	2.6769e+004	-
Uncertainty in load demand	1.4636e+005	1.5323e+004
Uncertainty in ambient temperature	4.8056e+004	2.2806e+003
Uncertainty in wind speed and power	6.5395e+004	1.9002e+002
Uncertainty	6.6566e+004	6.7159e+002

Table III. Mean and standard deviation of the EENS for the deterministic base case and the four uncertain scenarios for the three load levels in Table II.

Table III shows that the increase of the load level produces an increase in the system annual energy losses, both for the deterministic base case scenario and for scenarios that include uncertainties. When the load level is less than or equal to 1.3 p.u., the system experiences no power loss in the deterministic base case scenario. In particular, when the system assumes the lowest load level (1.3 p.u.), the major contribution to the annual power losses is determined by uncertainties in wind speed and wind power production. For larger load level values, i.e. 1.4 p.u and 1.5 p.u., uncertainties in the load demand cause the largest losses. Since stochastic simulations are considered over 100 years, it can be expected that the size of the energy losses that are registered in each year may vary consistently. Nonetheless, in all the scenarios, the standard deviation value of the EENS is one to two orders of magnitude smaller than its mean value. It is worth noting that scenario IV, that combines the effects of all the uncertainties, experiences an average EENS smaller than the average EENS of scenarios in which the different uncertainties are propagated separately. This is an effect of compensation of the uncertainties that lowers the average energy not served to the customers when considering the simultaneous impact of all the different sources of uncertainty.

In the following analysis, attention is focused on the largest load level value (1.5 p.u) because it is a good paradigm for systems with a high degree of utilization which operate in stress conditions, and represents the worst-case scenario in terms of energy not supplied. Figure 9 shows the impact that all the identified uncertainties have on the power grid when load level is 1.5 p.u., quantified in terms of power loss. These estimates are average values based on 100 samples, i.e. 100 years of system operations were simulated for each scenario that includes uncertainties. The power loss is quantified by the Expected Demand Not Supplied, i.e. the average EDNS index for each hour of the year. The EDNS index is an adequacy index for the transmission level of the electric infrastructure [2]. It quantifies the power not supplied to the network and it is a suitable index when dealing with events. From Figure 9, it can be noticed that power losses occur in a burst fashion during the year, with two loss peaks occurring at the very beginning of the year and in summer; the highest peak load occurs in the week prior to the end of the year. In order to understand this behavior, the EDNS is compared to the hourly peak load curve (inset in Figure 9), which represents the seasonal load profile of system users. In the simulation, it is assumed that the first hours in the hourly peak load curve correspond to the first hours of the calendar year. It can be noticed that the highest values in EDNS corresponds to the periods in the year where power requests reach the peak value.

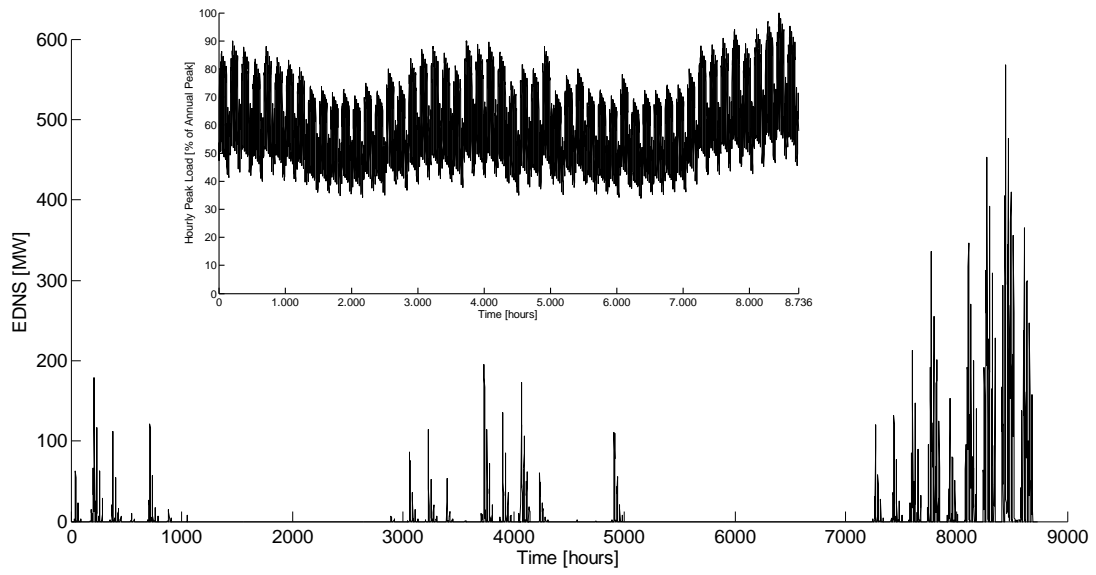


Figure 9. Representation of the hourly average loss of power due to uncertainties for the load level = 1.5. The average is considered over a period of 100 years. The inset represents the hourly peak load curve: the highest losses correspond to the highest demand from the consumers.

In order to understand the causes for the demand not supplied in Figure 9 and to devise operational safety margins which could prevent the occurrences of these losses, the global system parameter that guides the flow pattern in the system, i.e., the total load requested at all the buses, **is investigated**. In Figure 10, the EDNS index is expressed as function of the total load requested at all the buses. It shows that there are small power losses, on average, until the demanded load reaches a threshold value of 3600 MW. Above the threshold value, the system loses power proportionally to the increasing load demand (Figure 10).

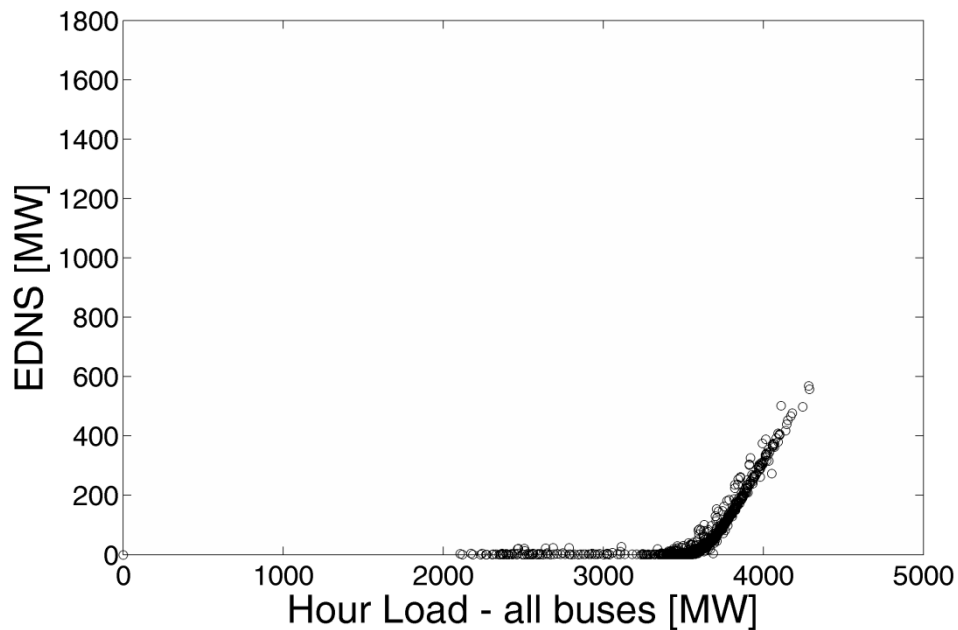


Figure 10. Average power loss as a function of the overall demanded load at all the buses. Each point is an average value evaluated in 100 simulated years

The EDNS index captures the average power losses. It may be expected that there will be years with very few losses and years where losses are significant; rare events, such as cascades, may pass unnoticed in an average analysis. Therefore, the contribution to power losses of every hour load of each year of simulation is considered (Fig. 11). The obtained Demand Not Supplied reveals that the majority of losses take place when hour loads values are around or exceed the threshold value of 3600 MW (bottom right of Figure 11).

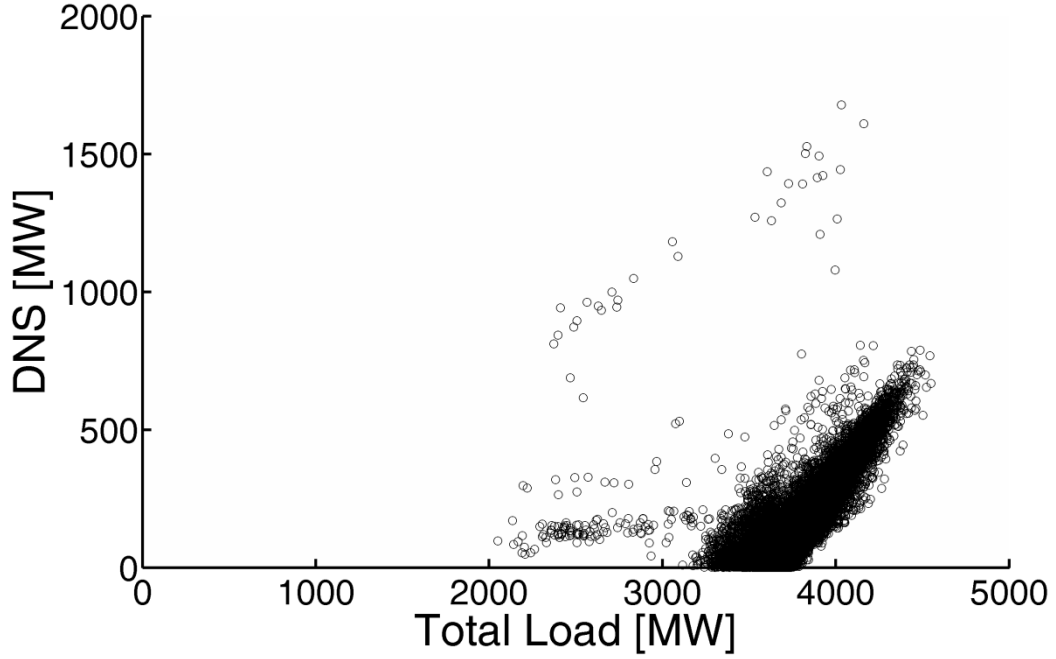


Figure 11. Hourly power loss as a function of the overall demanded load at all the buses

Nevertheless, the overall load requests alone cannot explain the magnitude of the demand not served. Indeed, some load demands may cause huge power losses as can be seen in Figure 11 (points at the top left and right), some other parameter must also influence the magnitude of the losses. Power loss values and power request values seem to subdivide the plane into the four quadrants detailed in Table IV.

	DNS [MW]	Hour Load [MW]
Quadrant 1	> 600	< 3200
Quadrant 2	< 600	< 3200
Quadrant 3	< 800	> 3200
Quadrant 4	> 800	> 3200

Table IV. Subdivision of the Cartesian plane in Figure 11 into 4 quadrants

Quadrants 1 and 2 encompass the same hour load range, but different power loss range and so do quadrants 3 and 4. Quadrants 1 and 4 register the highest losses.

In order to understand which uncertain parameters affect the power losses in the transmission network, the cumulative distribution functions for ambient temperature, wind speed and wind power output in the four quadrants are represented in Figures 12-14.

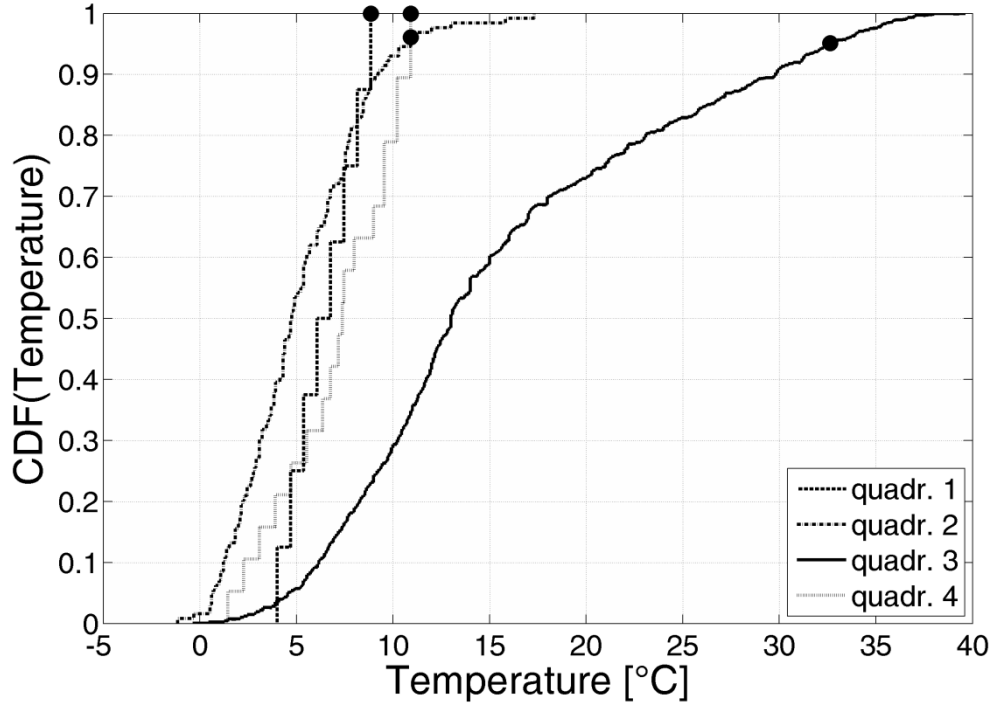


Figure 12. Cdf of ambient temperature distributions in the 4 quadrants. The black points represent the 95th percentile of each cdf.

In Figure 12, the 95th percentile of each cdf is represented by a black point. Three of the four cumulative distributions of ambient temperature concentrate at low temperatures values, between 8°C and 11°C. These cdfs correspond to quadrants 1, 2 and 4 (Table IV): the large power losses (quadrants 1 and 4) occur during winter season, when also small losses occur (quadrant 2). It seems reasonable to exclude that hot ambient temperature contributes to the overheating of the transmission lines. Indeed, the cdf of quadrant 3 includes the majority of small losses which occur throughout the year: the temperature values for the cdf range from typically winter ambient temperature values, next to 0°C, to summer hot ambient temperature values above 35°C.

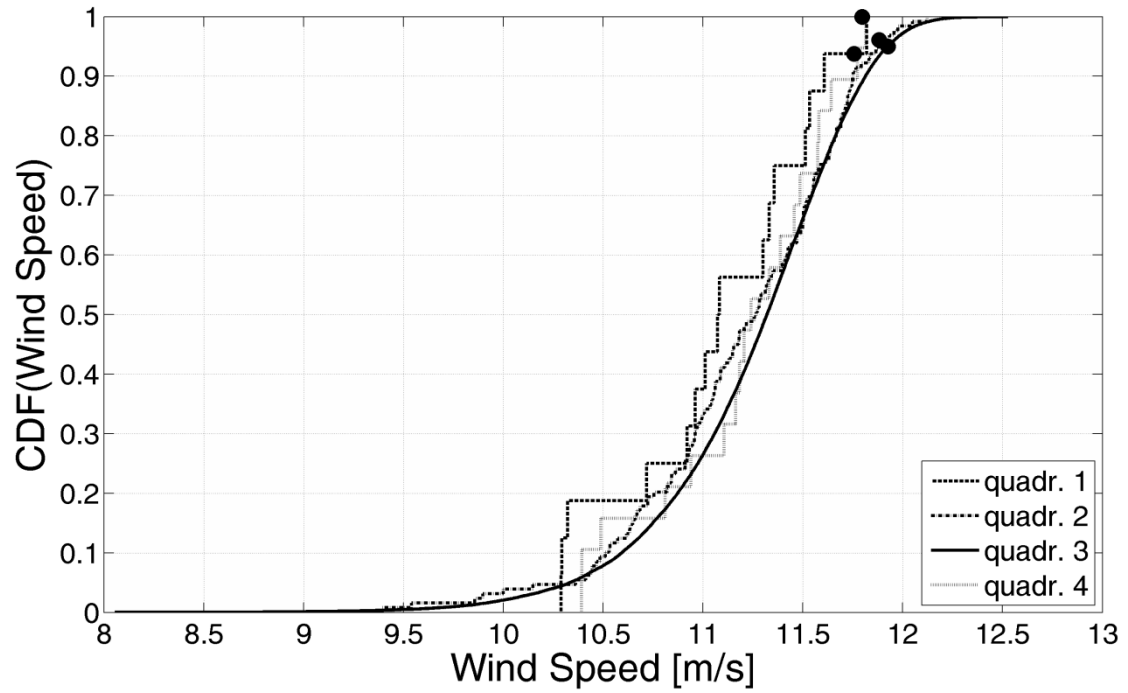


Figure 13. Cdf of wind speed distributions in the four quadrants. The black points represent the 95th percentile of each cdf.

Figure 13 represents the cumulative wind speed distributions. The 95th percentile values concentrate in a very small range of wind speed values, between 11.7 ms^{-1} and 11.9 ms^{-1} . The uncertainty associated to the cooling of the overhead line does not contribute to the power losses.

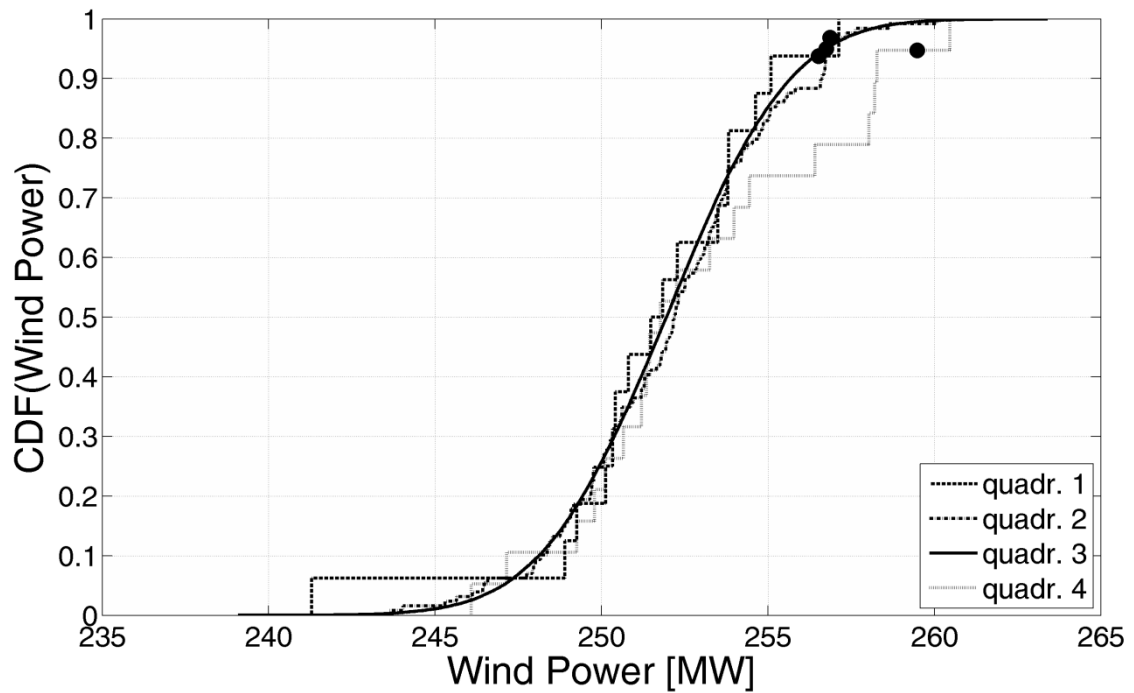


Figure 14. Cdf of wind power generation distributions in the four quadrants. The black points represent the 95th percentile of each cdf.

Figure 14 shows the cumulative distribution for the wind power generation. The cumulative distributions related to wind speed and wind power distribution show similar trends in the four quadrants, although the 95th percentile value corresponding to quadrant 4 is larger if compared to the other three 95th percentiles.

From Figures 12-14, **it can be concluded** that no single parameter affects the magnitude of the power losses. Therefore, the combined effects of multiple system parameters on the power losses **are investigated**.

Cascades in the grid are triggered by overloaded lines: once a transmission line reaches the limit temperature (T_{cl}), the line is disconnected from the grid for a fixed amount of time during which its temperature drops under the T_{cl} value. The transmission lines that disconnect with larger frequency are line 25, line 26 and line 28; as can be seen in Figure 7, these lines connect the upper four buses, i.e. bus 17, 18, 21, 22, with the rest of the network.

If the unavailability of a transmission line **is defined** as the percentage of time during the year that the line is disconnected from the system, **it can be seen** from Table V that, on average, line disconnections last longer when load levels are higher.

	Unavailability (Load level = 1.3)	Unavailability (Load level = 1.4)	Unavailability (Load level = 1.5)
Line 25	0.0795	0.2109	0.3452
Line 26	0.2557	0.4188	0.5664
Line 28	0.0790	0.1969	0.3262

Table V. Unavailability of the disconnected lines for the different load levels of demand.

The disconnection frequency analysis reveals that the modified system with load level = 1.5 p.u. is highly stressed and it experiences a random sequence of disconnections of lines 25, 26, 27. When they are simultaneously disconnected, the system divides in two parts: an upper island including buses 17, 18, 21, 23 and a lower island composed by the remaining 20 buses (Fig. 7).

In the first island, composed by the upper part of the network, there are two generating buses, i.e. bus 21 and bus 22, that supply the only load bus left, i.e. bus 18: no losses or further disconnections are registered and the generation dispatch guarantees a balanced power supply in the island.

On the other hand, the lower part of the network has many load buses and a generating system that is not fit to supply enough power in response to the variable load demand. When requested loads in the sub-system reach large values, the demand cannot always be supplied by the generating units and some power demand cannot be served.

In 100 years of simulation, the behavior of the system has been analyzed and attention has been focused on the same hours of the years when cascades occur only in year 30 and year 98, and on the same hours of years when no contingencies take place; years 2, 14, 31, 42, 54 were taken as examples.

The starting event for the cascades is the disconnection of line 18 always occurring at hour 8443 of the year; then, lines 20, 21, and 29 disconnect in sequence, subdividing the lower part of the MRTS system in two smaller islands where other disconnections occur propagating the cascade all through the lower sub-system. Figure 15 shows that load demand in the hour during which the cascade occur, i.e. hour 8443, is large in year 30 and year 98, when the cascade occurs, but the power request is large also for the same hour in year 14 and year 42 when no cascade takes place.

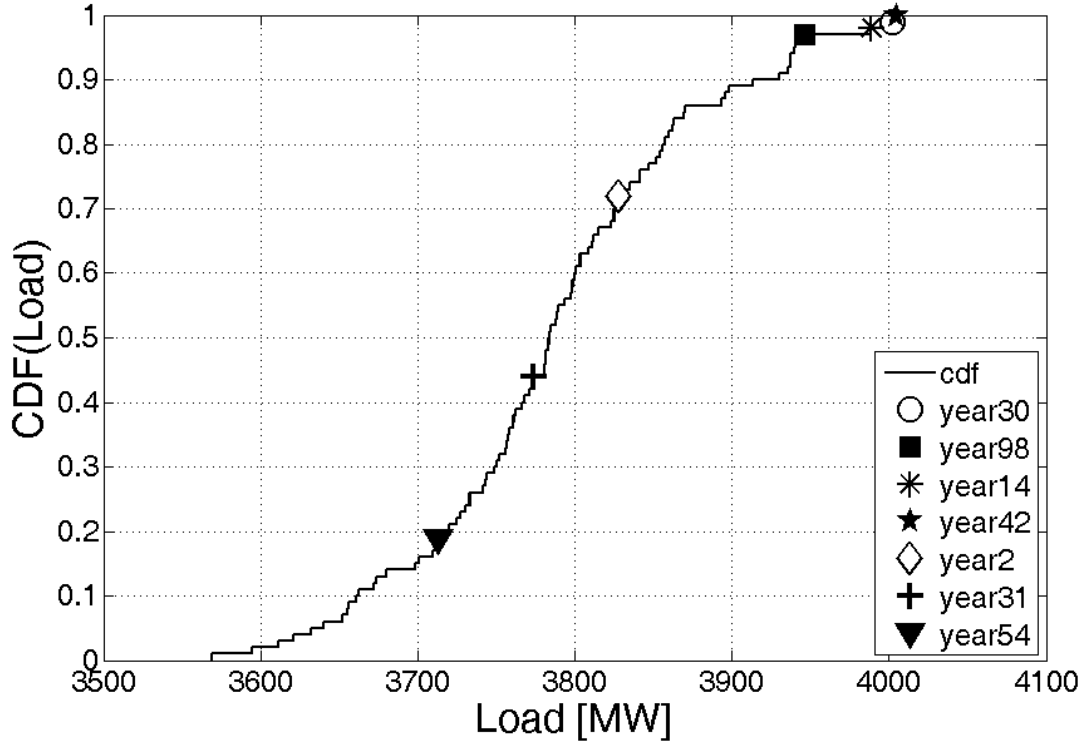


Figure 15 Cumulative distribution function of load demand at hour 8443.

Yet, from Figure 16, it can be noticed that in correspondence of years 14 and 42, wind power generation at buses 1 and 3 is larger than it is in years 30 and 98, when cascades occur.

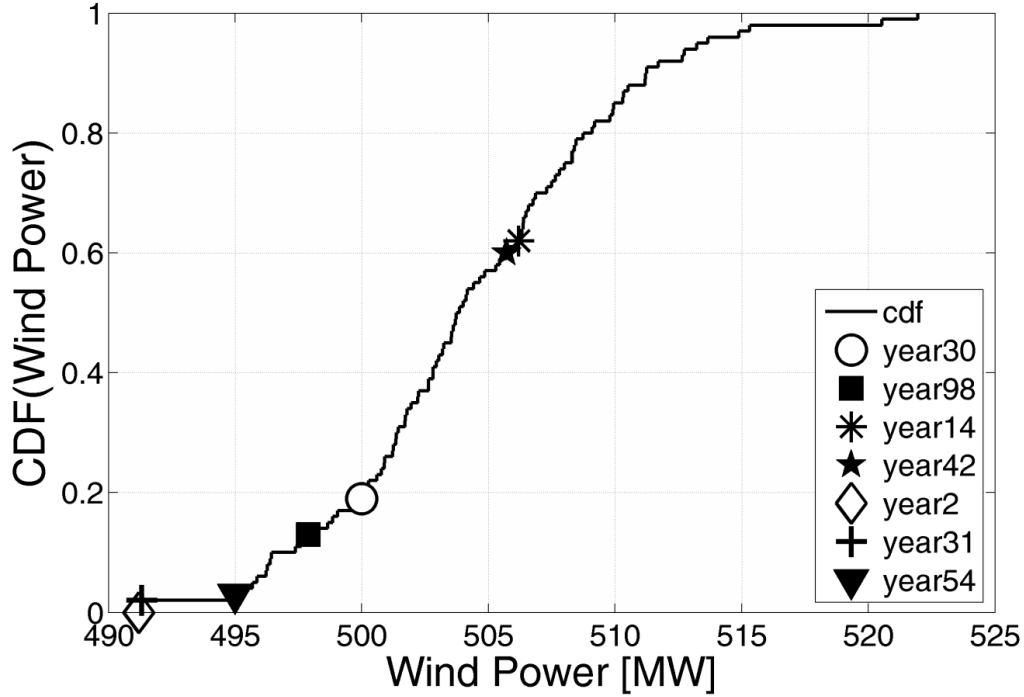


Figure 16. Cumulative distribution function for wind power output at hour 8443.

By the same token, years 2, 31 and 54 record a lower wind generation output than years 30 and 98 (Figure 16) but no contingencies occur because the corresponding load demand is small (Figure 15).

Therefore, uncertainties in the wind conversion system may prevent the transmission in the power grid causing cascades. The DNS values in quadrants 2 and 3 are due to the lack of adequacy of the lower island, i.e. the generation cannot match the demanded power in hours of large power requests. Conversely, the DNS values in quadrants 1 and 4 are due to the incapability of the generated power of reaching the load buses, due to a cascade of line disconnections that isolates almost completely every load bus in the lower part of the network. The cascade of line disconnections is triggered by spatial unbalance between power requests and power generation, namely the wind power generation at buses 1 and 3 is not capable of meeting the local power request and power has to flow from the upper right part of the lower island causing line disconnection.

The interplay between wind power generation and overall power request in the lower island constitutes a probabilistic safety margin which has to be monitored in order to avoid line disconnection cascade propagation and to limit the demand not supplied by the customers.

5. Conclusions

The issue of the uncertainty in composite generation and transmission networks incorporating large-scale wind energy facilities and developed a simulation framework of analysis has been addressed. Wind speed variability, wind power variability, ambient temperature variability and load variability have been considered. As test-bed for the exemplification of the framework, a transmission-deficient setting has been created in the MRTS by increasing the system load level and the generating capacity, to represent general conditions that exist in actual power systems. The impact that the identified uncertainties have on the reliability of the electric infrastructure has been quantitatively analyzed: variability in load and in wind power generation have the biggest impact on the system.

The following are some of the main findings of this application:

- The combined, simultaneous effect of all the different sources of uncertainty has a smaller impact on system safety in terms of expected energy not supplied, than individual uncertainty sources: this is an effect of compensation of the uncertainties, which lowers the average energy not served to the customers.
- The increase in the transmission system utilization can lead to cascade events if wind power output cannot sustain the load demand. Indeed, large power requests in the system cause the disconnections of the lines that link the upper part of the network, in which massive generating units are concentrated, and the lower part of the network, thus preventing the power transfer to the area with the highest concentration of buses. When the system tears apart, power request must be supplied by local power generation. In this situation, wind power generation may not be capable of satisfying the local power request causing cascade events of power line disconnections.
- More generally, the interaction between wind power generation and the overall power request serves as paradigm for the assessment of the safety margins of the system, because no single parameter affects the magnitude of the power losses.

References

- [1] W. Kroger, E. Zio, *Vulnerable System*, Springer, London, 2011.
- [2] R. Billinton, W. Li, *Reliability Assessment of Electric Power Systems Using Monte Carlo Methods*, New York Plenum Press, (1994), pp.229-308.
- [3] M. Ivey, A. Akhil, D. Robinson, K. Stamber, J. Stamp, Consortium for Electric Reliability Technology Solutions Grid of the Future White Paper on Accommodating Uncertainty in Planning and Operations, Prepared for the Transmission Reliability Program Office of Power Technologies Assistant Secretary for Energy Efficiency and Renewable Energy U.S. Department of Energy, 1999.
- [4] NERC North American Electric Reliability Corporation, *Special Report: Accommodating High Levels of Variable Generation*, April 2009.
- [5] M. Xu, X. Zhuan, Optimal planning for wind power capacity in an electric power system, *Renewable Energy*, Vol. 53, (2013), pp. 280-286.

- [6] E.K. Hart, M.Z. Jacobson, A Monte Carlo approach to generator portfolio planning and carbon emissions assessments of systems with large penetrations of variable renewables, *Renewable Energy*, 36, (2011), pp. 2278 – 2286.
- [7] Y. Li, E. Zio, Uncertainty analysis of the adequacy assessment model of a distributed generation system, *Renewable Energy*, 41 , (2012), pp. 235 - 244.
- [8] M.A. Abdullah, A.P. Agalgaonkar, K.M., Muttaqi, Probabilistic load flow incorporating correlation between time-varying electricity demand and renewable power generation, *Renewable Energy*, 55, (2013) pp.532-543.
- [9] Y. Ding, P. Weng, L. Goel, P.C. Loh, Q. Wu, Long-term reserve expansion of power systems with high wind power penetration using universal generating function methods, *IEEE Transactions on Power Systems*, Vol. 26, No.2, (2011), pp.766-774.
- [10] C. Grigg, P. Wong, et al., The IEEE Reliability Test System-1996. A report prepared by the Reliability Test System Task Force of the Application of Probability Methods Subcommittee, *IEEE Transactions on Power Systems*, Volume 14, Issue 3, (1999), pp:1010–1020.
- [11] I. Dobson, B.A. Carreras, V.E. Lynch, D.E. Newmann, An initial model for complex dynamics in electric power systems blackouts, *Hawaii international Conference on System Sciences*, January, 3-6, Maui, Hawaii, 2001.
- [12] M. Anghel, M., A.K. Werley, A.E. Motter, Stochastic Model for Power Grid Dynamics, *Proceedings of the 40th Hawaii International Conference on System Sciences*, 2007.
- [13] P. Giorsetto, K.F. Utsurogi, Development of a new procedure for reliability modeling of wind turbine generators, *IEEE transaction on Power Apparatus and Systems*, Vol. PAS-102, No.1, January, 1983.
- [14] A.J. Wood B.F. Wollenberg, *Power Generation, Operation, and Control*, 2nd ed. John Wiley & Sons, New York, 1996.
- [15] L.L. Grigsby, *Power System*, CRC press, Taylor and Francis Group LLC, 2007.
- [16] H. S. Carslaw and J. C. Jaeger, *Conduction of Heat in Solids*, 2nd ed. Clarendon Press, Oxford, 1959.
- [17] T. Ackermann, *Wind Power in Power Systems*, Jonn Wiley and Sons Ltd, West Sussex, England, 2005.
- [18] R. Billington, D. Huang, Aleatory and Epistemic Uncertainty Considerations in Power System Reliability Evaluation, Probabilistic Methods Applied to Power Systems. PMAPS '08. *Proceedings of the 10th International Conference on*, 25-29 May 2008.
- [19] F.O. Hoffman, J.S. Hammonds, *Propagation of Uncertainty in Risk Assessments: The Need to Distinguish Between Uncertainty Due to Lack of Knowledge and Uncertainty Due to Variability*, Risk Analysis, Vol. 14, No. 5, (1994) pp. 707-712.
- [20] G.E. Apostolakis, The concept of probability in safety assessments of technological systems. *Science*, 250(4986), (1990), pp.1359–1364.
- [21] M.A. Matos, E.M. Gouveia, The Fuzzy Power Flow Revisited. *IEEE Transactions on Power Systems*, 23(1), (2008), pp.213 - 218.

- [22] E.M. Gouveia, M.A. Matos, Symmetric ac fuzzy power flow model, *European Journal of Operational Research*, 197(3), (2009), pp. 1012–1018.
- [23] R. Billinton, Y. Gao, Adequacy assessment of composite power generation and transmission systems with wind energy, *International journal of Reliability and Safety*, vol. 2, No. 1, (2008), pp.79-98.
- [24] R. Karki, R. Billinton, Incorporating wind power in generating system reliability evaluation, *Int Journal of system assurance Engi. Manag*, 2, (2010), pp. 120-128.
- [25] G.K.Johnson, *Wind Energy systems*, Electronic edition, 2006.
- [26] B. Safari, J. Gasore, A statistical investigation of wind characteristics and wind energy potential based on the Weibull and Rayleigh models in Rwanda, *Renewable Energy*, vol. 35, (2010), pp. 2874-2880.
- [27] A.M. Foley, P.G. Leahy, A. Marvuglia, E.J. Mckeogh, Current methods and advances in forecasting of wind power generation, *Renewable Energy*, 37, (2012), pp. 1-8.
- [28] J.G. Sloomweg, W.L. Kling, Modeling of large wind farms in power system simulations, *IEEE Proc.-c, Power Engineering*, (2002), pp.503-508.
- [29] T. Thiringer, J. Linders, Control by variable rotor speed of a fixed-pitch wind turbine operating in a wide speed range, *IEEE Transaction on Energy Conversion*, vol. 8, no. 3, (1993), pp. 520-526.
- [30] T. Jin, Z. Tian, Uncertainty Analysis for Wind Energy Production with Dynamic Power Curves, *IEEE 11th International Conference on Probabilistic Methods Applied to Power Systems (PMAPS)*, San Marcos, TX, USA, 14 - 17 june 2010.
- [31] R. Billinton, Y. Gao, R. Karki, Composite System Adequacy Assessment Incorporating Large Scale Wind Energy Conversion Systems, Considering Wind Speed Correlation, *IEEE Transaction on Power Systems*, Vol. 24, No.3, August 2009.